Inorganic Chemistry

ARTICLE

pubs.acs.org/IC

Combined Experimental and Computational Study of *cis-trans* Isomerism in Bis(L-valinato)copper(II)

Marijana Marković,[†] Nenad Judaš,[‡] and Jasmina Sabolović*[,†]

[†]Institute for Medical Research and Occupational Health, Ksaverska cesta 2, P.O. Box 291, HR-10001 Zagreb, Croatia

[‡]Laboratory of General and Inorganic Chemistry, Department of Chemistry, Faculty of Science, University of Zagreb, Horvatovac 102a, HR-10000 Zagreb, Croatia

Supporting Information

ABSTRACT: Heating of polycrystalline *cis* aquabis(L-valinato)copper(II) at 90 °C resulted in a dehydrated powder. Recrystallization from aqueous solution of the obtained product yielded anhydrous *trans* bis(L-valinato)copper(II). The X-ray crystal and molecular structures of *trans* bis(L-valinato)copper(II) and *cis* aquabis(L-valinato)copper(II) are presented. Molecular modeling calculations were attempted to resolve factors that influenced the isomerization and crystallization of either the aqua *cis*- or the anhydrous *trans*-isomer. Conformational analyses of *trans*- and *cis*-isomers were completed in vacuo and in crystal by molecular mechanics, and in aqueous solution by molecular dynamics (MD) simulations using the same force field. Although the conformers with *trans*-configuration are the most stable in vacuo, those with *cis*-configuration form more favorable intermolecular interactions. Consequently, both *cis*- and *trans*-isomers are predicted to be present in aqueous solution. According to the crystal structure simulations and predictions, *cis*-isomer requires water molecules to form energetically more stable crystal packings than *trans*-isomer. The MD modeling of the self-assembly of 16 bis(L-valinato)copper(II) complexes in aqueous solution for the first time predicted the crystallization nucleus formation to proceed from monomers to oligomers by Cu-to-$O_{carboxylato}$ and/or $N-H\cdots O_{carboxylato}$ weak bonds; these oligomers then bind together via water molecules until they acquire the right positions for noncovalent bonding like in the experimental crystal structures. Fifty-nanosecond MD simulations accomplished for a system consisting of equal numbers of complexes and water molecules at 298 and 370 K suggested complete *cis*-to-*trans* transformation at the higher temperature. Prevalence of either *cis*- or *trans*-conformers in water upon dissolvation may explain the crystallization results.

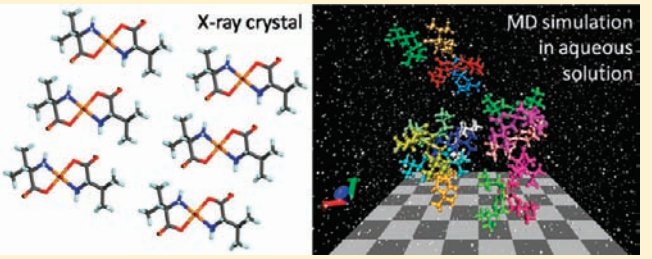

INTRODUCTION

Copper(II) amino acid complexes have been known since the second half of the 19th century; however, their intensive structural studies, motivated by the fact that they could be appropriate model compounds for copper-binding sites in copper-containing metalloproteins, started in the 1960s.[1] A survey of the Cambridge Structural Database (version 5.31, update of August 2010) completed using ConQuest[2] (version 1.12) and limited to bis(amino acidato-*N,O*)copper(II), $Cu(aa)_2$, complexes with determined atomic coordinates and *R*-factor ≤0.20 revealed 122 entries. Among them, 28 belonged to copper(II) complexes with glycine and optically pure standard α-amino acids in a nonionic crystal structure, and represented only 10 and 8 different *trans* and *cis* complexes, respectively.[3]

$Cu(aa)_2$ complexes can be considered as polyfunctional and polytopic molecules because of their intermolecular bonding properties. Mononuclear complexes are bonded into one-dimensional (1D), two-dimensional (2D), or three-dimensional (3D) solid-state architectures by noncovalent interactions (e.g., hydrogen bonds formed by the amino and carboxylate groups; aliphatic-aliphatic van der Waals interactions formed by the α-amino acid residues). Usually copper(II) coordination is completed by weak apical coordinative bonding of either a water oxygen atom or a carbonyl oxygen atom from an adjacent molecule. Truly four-coordinate copper(II) was found in the crystal structures of copper(II) *N,N*-dialkylated amino acidates.[4−8] Moreover, additional building blocks for supramolecular structures are provided by the phenomenon of *cis-trans* isomerism. Unfortunately, little control has been attained over *cis-trans* isomerism during crystallization.[9]

Although measurements of infrared (IR) spectra[10] and diffuse reflectance spectra[11] enabled identification of *trans* and *cis* $Cu(aa)_2$ complexes in powdered samples, the crystal and molecular structures of both isomers were determined in only a few cases because of the difficulty to find proper conditions for obtaining single crystals. These are *cis* and *trans* copper(II) complexes with glycine,[12−14] L-alanine,[15,16] and 1-aminocyclopropane carboxylic

Received: December 30, 2010
Published: March 21, 2011

acid.[17] Bis(glycinato)copper(II) hydrate, $Cu(Gly)_2 \cdot H_2O$, crystallized from aqueous solution as a *cis* isomer,[12,13] but bis(L-alaninato)copper(II) crystallized as an anhydrous *trans* isomer.[15] The single crystals of *trans* $Cu(Gly)_2$ were grown from aqueous solution saturated with the excess of glycine.[14] Anhydrous *cis* bis(alaninato)copper(II) single crystals were obtained from initially synthesized *trans* isomer by shaking of the saturated solution,[18] and by heating of the aqueous suspension.[16] The copper(II) complex with 1-aminocyclopropane carboxylic acid has a unique crystal phase built of trimeric units composed of one *trans* and two *cis* molecules.[17]

In this Article we present a new crystal and molecular structure of a $Cu(aa)_2$ complex: anhydrous *trans* bis(L-valinato)copper(II), $Cu(L\text{-}Val)_2$. To compare the crystal structures of the geometric isomers, we have also redetermined the crystal and molecular structure of *cis* aquabis(L-valinato)copper(II), $Cu(L\text{-}Val)_2 \cdot H_2O$.[19−22]

In the solid state, Delf et al. studied the thermal *cis*−*trans* interconversion mechanism that occurred upon heating of $Cu(Gly)_2$ at a temperature higher than 100 °C, from hydrated *cis*-isomer to thermodynamically more stable anhydrous *trans*-isomer.[23] Similar thermal solid state *cis*-*trans* rearrangements in coordination compounds[24] occurred for, for example, $[CrCl_2trimethylenediamine_2]Cl$ at 160−209 °C,[25] $[CoX_2ethylenediamine_2]X$ (X = Cl or Br) at 210−215 °C,[26] and dihalogenbis(trialkyl (or aryl)phosphine)Pt(II) practically in the melt.[27]

The stability constant measurements of the copper(II) chelates with aliphatic α-amino acids yielded $Cu(aa)_2$ complexes as the predominant species in aqueous solutions at ambient temperatures.[28−30] *Trans* and *cis* isomers for many $Cu(aa)_2$ complexes were identified to simultaneously exist in aqueous solutions by the ^{14}N superhyperfine structure in electron paramagnetic resonance (EPR) spectra.[31−34] Solvent composition can affect the *cis*−*trans* equilibrium as revealed by the EPR spectra of $Cu(L\text{-}Val)_2$ studied as a function of the dioxane to D_2O solvent composition ratio, that the addition of dioxane induced a shift toward the *trans* isomer.[33] Low-molecular-weight copper(II) complexes with amino acids and peptides mediate copper transport and storage in biological fluids,[35] and *cis*−*trans* isomerism may have an important role in these processes.

The high-level molecular quantum mechanical (QM) calculations of the *cis*-*trans* isomerization reaction for $Cu(Gly)_2$ showed that in the gas phase and at ambient temperatures the energy barrier (29 kJ mol^{-1}) is low enough for a *cis*-isomer to spontaneously transform to a more stable *trans*-isomer (by 57 kJ mol^{-1}) via a chelate-ring twisting mechanism without breaking bonds.[36] Another possible *cis*−*trans* isomerization mechanism via a chelate-ring-opening was ruled out for being energetically too demanding.[36] Conversely to the gas phase, the QM calculations of $Cu(Gly)_2$ in water medium at 300 K using a polarized continuum model revealed a small energy difference (5 kJ mol^{-1}) between the solvated *cis* and *trans* minima, and a substantial increase of the potential energy barrier for *cis*-to-*trans* isomerization (70 kJ mol^{-1}).[37]

In an attempt to resolve the physicochemical mechanism which brought to crystallization either aqua *cis* or anhydrous *trans* isomer of $Cu(L\text{-}Val)_2$, and to contribute to the knowledge of factors influencing the *cis*-*trans* isomerism, we have undertaken molecular modeling calculations in vacuum, in crystalline surroundings, and in aqueous solution. These calculations were possible thanks to the molecular mechanics (MM) force field FFWa-SPCE[37] suited for the MM and molecular dynamics (MD) simulations of *trans* and *cis* $Cu(aa)_2$ complexes in different environments by explicit accounting for the surroundings effects such as crystal lattice or aqueous solution.[37,38] In this study we combined the experimental X-ray data and the MM and MD simulation results to decipher the isomerization and crystallization processes occurring at the molecular level upon recrystallization of the initially synthesized and thermally treated powdered samples of $Cu(L\text{-}Val)_2$ from aqueous solution.

Table 1. Crystallographic Data for *trans* $Cu(L\text{-}Val)_2$ and *cis* $Cu(L\text{-}Val)_2 \cdot H_2O$

	trans $Cu(L\text{-}Val)_2$	*cis* $Cu(L\text{-}Val)_2 \cdot H_2O$
empirical formula	$C_{10}H_{20}N_2O_4Cu$	$C_{10}H_{22}N_2O_5Cu$
formula weight (g mol^{-1})	295.84	313.84
crystal system	triclinic	monoclinic
crystal size (mm^3)	0.61 × 0.56 × 0.23	0.73 × 0.54 × 0.13
crystal habitus	prismatic	prismatic
crystal color	blue-violet	blue
space group	*P*1	*C*2
a (Å)	4.905(1)	21.348(1)
b (Å)	5.242(1)	9.589(2)
c (Å)	12.213(1)	7.425(2)
α (deg)	79.36(1)	90
β (deg)	89.84(1)	108.91(2)
γ (deg)	79.42(1)	90
volume ($Å^3$)	303.21(4)	1437.85(5)
Z	1	4
D_{calc} (g cm^{-3})	1.620	1.450
μ (mm^{-1})	1.81	1.53
F(000)	155	660
Flack parameter	0.031(8)	−0.003(15)
reflections collected/unique	2770/2766	2469/2430
data/restraints/parameters	2766/7/174	2468/26/244
goodness-of-fit on F^2, S^a	1.049	1.040
R/wR [$I > 2\sigma(I)$]^b	0.0181/0.0513	0.0326/0.0793
largest diff. peak and hole (e $Å^{-3}$)	0.240, −0.379	0.501, −0.348

$^a S = \Sigma[w(F_o^2 - F_c^2)^2/(N_{obs} - N_{param})]^{1/2}$. $^b R = \Sigma||F_o| - |F_c||/\Sigma F_o$, $w = 1/[\sigma^2(F_o^2) + (g_1P)^2 + g_2P]$ where $P = (F_o^2 + 2F_c^2)/3$; $wR2 = [\Sigma(F_o^2 - F_c^2)^2/\Sigma(F_o^2)^2]^{1/2}$.

EXPERIMENTAL SECTION

Synthesis of $Cu(L\text{-}Val)_2$ and Single-Crystal Preparations. *Materials.* Copper(II) chloride dihydrate (Merck, Darmstadt, Germany) and L-valine (Dr. Th. Schuchardt & Co., Hohenbrunn, Germany) were used without further purification. Deionized water was produced in laboratory.

Synthesis of cis $Cu(L\text{-}Val)_2 \cdot H_2O$. According to the published method,[39] we mixed 26 mL of 0.2 M $CuCl_2 \cdot 2H_2O$ solution (0.900 g, 5.278 mmol) with L-valine (1.500 g, 12.804 mmol) dissolved in 10 mL of 1 M NaOH water solution. The reaction mixture was left for 2 days at room temperature. The resulting blue powder of *cis* $Cu(L\text{-}Val)_2 \cdot H_2O$ was filtered off, dried, and weighed (yield: 75.1%). Blue plate-like single crystals of *cis* $Cu(L\text{-}Val)_2 \cdot H_2O$ were obtained during recrystallization (i.e., 0.125 g of complex powder was dissolved in 10 mL of deionized water) by slow evaporation at room temperature.

Crystallization of trans $Cu(L\text{-}Val)_2$. The initially synthesized blue powder of *cis* $Cu(L\text{-}Val)_2 \cdot H_2O$ was heated for 24 h at 90 °C (the weight

dx.doi.org/10.1021/ic102585f |*Inorg. Chem.* 2011, 50, 3632–3644

loss percentage of 5.9% corresponded to one water molecule loss per Cu(L-Val)$_2$ molecule). The resulting solid phase (0.125 g) was dissolved in 10 mL of deionized water. After a few days tiny blue aggregations appeared in the solution, and after a few weeks blue-violet needle-like single crystals of the anhydrous *trans* Cu(L-Val)$_2$ isomer crystallized on the vessel walls and were used in the X-ray diffraction experiment.

X-ray Diffraction Experiments. The single-crystal X-ray data of *trans* Cu(L-Val)$_2$ and *cis* Cu(L-Val)$_2$·H$_2$O were collected on an Oxford Diffraction Xcalibur CCD diffractometer with graphite-monochromated MoKα radiation at room temperature. All the data were collected using ω-scans. Table 1 presents details of data collection and crystal structure refinement. CrysAlis CCD and CrysAlis RED programs[40] were employed for data collection, cell refinement, and data reduction. The structures were solved by direct methods. The refinement procedure by full-matrix least-squares methods based on F^2 values against all reflections included anisotropic displacement parameters for all non-H atoms.

The *iso*-propyl moiety in *cis* Cu(L-Val)$_2$·H$_2$O was disordered over two sites with relative population parameters 0.60 and 0.40. The bond distances between the disordered atom pairs C13A and C14A, C13A and C15A, as well as C13B and C14B, C13B and C15B were set to 1.520 Å (s.u. 0.008 Å), using the DFIX command. The same procedure was applied for the disordered atom C25 to atom C23 bond distances. Finally, the disordered carbon atoms were refined using a restrained anisotropic model achieved (the ISOR command). The positions of the hydrogen atoms of the NH$_2$ groups and water molecules were determined from the difference Fourier map and were included in the refinement process with an isotropic thermal parameter. Other hydrogen atoms were positioned geometrically and refined applying the riding model [C−H = 0.95−0.98 Å and with U_{iso}(H) = 1.2 or 1.5U_{eq}(C)]. All calculations were performed using SHELXS97[41] and SHELXL97[42] (within the WinGX program package).[43] Molecular graphics were done using ORTEP,[44] Mercury,[45] RASTOP[46] and POVRay.[47]

X-ray powder diffraction (PXRD) experiments were performed on a Philips PW3710 diffractometer using CuKα radiation, with a zero background sample holder in the Bragg−Brentano geometry; tension 40 kV, current 40 mA. The patterns were collected in the angle region between 4° and 40° (2θ) with a step size of 0.02° and 1.0 s counting per step. The data were collected and visualized using the X'Pert programs suite.[48]

Thermal Measurements. Thermogravimetric (TG) analyses were performed on a Mettler-Toledo TGA/SDTA851 thermobalance, and differential scanning calorimetry (DSC) measurements on a DSC325 calorimeter using aluminum crucibles under the stream of nitrogen (300 mL min^{-1}). Several experiments were made with different heating rates (0 or 10 K min^{-1}). The maximum temperature was 623 K. The results were processed with the Mettler STARe 9.01 software. PXRD patterns were collected for all the residues found in crucibles.

IR Spectroscopy. The IR spectra were recorded on an EQUINOX 55 FTIR spectrophotometer using a KBr pellet technique. The data collection and analysis were performed using the program package OPUS 4.0.[49]

trans Cu(L-Val)$_2$: 3291 cm^{-1} (s, br, ν_{N-H}); 3158 cm^{-1} (s, ν_{N-H}); 2955, 2935, and 2875 cm^{-1} (vs, s, and m, respectively, δ_{CH3}); 1623 and 1595 cm^{-1} (vs, overlapped, ν_{C-O} and $\nu_{C=O}$).

cis Cu(L-Val)$_2$·H$_2$O: 3284 cm^{-1} (s, br, ν_{N-H}); 3159 cm^{-1} (s, ν_{N-H}); 2967, 2933, and 2877 cm^{-1} (s, s, and m, respectively, δ_{CH3}); 1627 and 1585 cm^{-1} (vs, overlapped, ν_{C-O} and $\nu_{C=O}$).

Product obtained by thermal treatment of *cis* Cu(L-Val)$_2$·H$_2$O: 3297 cm^{-1} (vs, br, ν_{N-H}); 3265 cm^{-1} (vs, ν_{N-H}); 2963, 2912, and 2875 cm^{-1} (s, m, and m, respectively, δ_{CH3}); 1625 and 1587 cm^{-1} (vs, overlapped, with shoulders at 1662 and 1617 cm^{-1}, ν_{C-O} and $\nu_{C=O}$).

Molecular Modeling Methods. *MM Calculations.* All MM calculations were performed using the modified version[50] of the Lyngby version of the CFF program,[51−53] and the FFWa-SPCE force field[37] suited for modeling anhydrous and aqua Cu(aa)$_2$ complexes with a *trans*- or a *cis*-CuN$_2$O$_2$ coordination polyhedron. The FFWa-SPCE force field parametrization procedure of deriving a set of empirical parameters equally applicable for vacuum, crystal, and aqueous solution was described elsewhere.[37] FFWa-SPCE reproduced well the QM derived vacuum structures, the experimental crystal data, the flexibility (plasticity) of the copper(II) coordination polyhedron both in vacuo and in crystal, and the impact of the intermolecular interactions on the geometry changes of a series of anhydrous and aqua *trans* and *cis* copper(II) amino acidates.[37] The force field reproduced qualitatively well relative stabilities of the QM vacuum structures.[37,54]

The conformational (strain) potential energy was calculated from the following basic formula:

$$\begin{aligned} V_{strain} &= V(b) + V(\theta) + V(\varphi) + V(\chi) + V_{LJ} + V_{Coulomb} \\ &= \sum_{bonds} D_e(e^{-2\alpha(b-b_0)} - 2e^{-\alpha(b-b_0)} + 1) \\ &\quad + \frac{1}{2}\sum_{valence\ angles} k_\theta(\theta-\theta_0)^2 + \frac{1}{2}\sum_{torsion\ angles} V_\varphi(1 \pm \cos n\varphi) \\ &\quad + \frac{1}{2}\sum_{out\text{-}of\text{-}plane\ angles} k_\chi\chi^2 + \sum_{i<j}(A_iA_jr_{ij}^{-12} - B_iB_jr_{ij}^{-6}) + \sum_{l<m} q_lq_mr_{lm}^{-1} \end{aligned}$$

Here b, θ, φ, χ, and r are the bond length, the valence, torsion, and out-of-plane angles, and the nonbonded distance, respectively. D_e, α, b_0, k_θ, θ_0, k_χ, V_φ, and n are the empirical parameters. One torsion per bond was calculated. A and B are one-atom empirical parameters of the Lennard-Jones 12−6 function, V_{LJ}. In the Lyngby-CFF program, the input charge parameters[8,37] are used for an assignment of fractional atomic charges, q, by a charge redistribution algorithm adjusted to assign the values close to those resulting from the natural population analysis (NPA) obtained for several anhydrous and aqua *trans* and *cis* Cu(aa)$_2$ systems.[54,55] The NPA charges for the Cu, N, and O atoms have very similar values in examined copper(II) chelates with natural α-amino acids.[54,55] Accordingly, the same and fixed fractional charge values were assigned for *cis* and *trans* Cu(L-Val)$_2$.[56] The intramolecular nonbonded interactions were calculated between the atoms separated by three or more bonds by the V_{LJ} and electrostatic, $V_{Coulomb,NB}$, potentials. In FFWa-SPCE,[37] the interactions inside the copper(II) coordination polyhedron are modeled using the Morse potential between the Cu and two amino N and two carboxylato O atoms, the repulsive electrostatic potential between these four donor atoms, $V_{Coulomb,1-3}$, and a torsion-like potential depending on the O−N−N−O "torsion" angle, with two minima corresponding to the *cis*- and the *trans*-planar CuN$_2$O$_2$ coordination geometries. The rationale for selecting these potential energy functions was described in our earlier papers.[8,54,55,57−59] Similar modeling of the valence angles around copper by the 1,3 donor−donor repulsions (but using the Buckingham or Lennard-Jones potentials), instead of using the valence-angle bending potential, is also present in other MM force fields developed for copper(II) and other transition metal complexes.[60−63]

The conformational potential energy was minimized for an isolated molecular system (in vacuo or a gas-phase approximation) and for a molecule surrounded by other molecules in a simulated crystal lattice. In vacuo, the minimum energy, V_{vacuum}, was calculated for two systems: Cu(L-Val)$_2$ (V_{vacuum} = V_{strain}), and Cu(L-Val)$_2$·H$_2$O (V_{vacuum} = V_{strain}[Cu(L-Val)$_2$] + V_{strain}[H$_2$O] + $V_{intermolecular}$). The interactions between the atoms of Cu(L-Val)$_2$ and the water molecule atoms, $V_{intermolecular}$, were modeled with the V_{LJ} and $V_{Coulomb,NB}$ potentials independently of the water molecule position around the complex.[54] The crystal simulations were performed using the Williams variant[64,65] of the Ewald lattice summation method with a spherical cutoff limit of 22 Å, and convergence constants of 0.2 Å^{-1}, 0.2 Å^{-1}, and 0.0 for Coulomb, dispersion, and repulsion lattice summation terms, respectively. The potential energy of an asymmetric unit in the simulated crystal environment, $V_{in\text{-}crystal}$, was calculated as the sum of the intramolecular strain

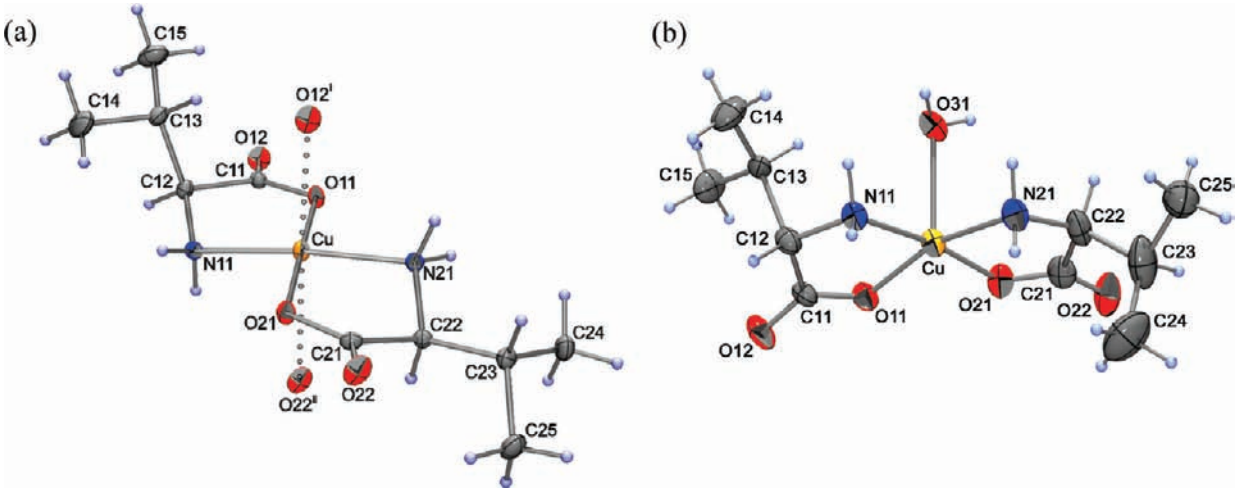

Figure 1. ORTEP-POV-Ray rendered view of (a) *trans* Cu(L-Val)$_2$ and (b) *cis* Cu(L-Val)$_2$·H$_2$O molecules. Ellipsoids are drawn at the 30% probability level. Hydrogen atoms are presented as spheres of arbitrary small radii. Disordered parts of the *cis* molecule were excluded from the drawing for clarity. Symmetry codes: $i = 1+x, y, z$; $ii = -1+x, y, z$.

potential energy, V_{strain}, and the intermolecular interactions (lattice energy), $V_{intermolecular}$, between the asymmetric unit atoms and the atoms of surrounding asymmetric units related by the space group symmetry operations and within the cutoff limit (i.e., $V_{in\text{-}crystal} = V_{strain} + V_{intermolecular}$). The intermolecular atom−atom interactions were calculated using the same functional forms and empirical parameters as for the intramolecular nonbonded interactions. During the in-crystal energy minimization, all atomic coordinates and unit cell dimensions were allowed to vary, except the α and γ unit cell angles were kept equal to 90° in the case of a monoclinic unit cell symmetry. The details of the in-crystal calculations are given elsewhere.[8,50,65]

MD Simulations. The simulations were performed using the program package Gromacs, version 3.2.1,[66,67] with the force field FFWa-SPCE.[37,56] The suitability of FFWa-SPCE for simulations and predictions in aqueous solution was examined for solvated *cis* and *trans* Cu(Gly)$_2$ [the only Cu(aa)$_2$ system for which some experimental structural data in aqueous solution at room temperature are available from the literature],[68] and additionally verified by comparison with the QM structural and energetic results obtained within the polarized continuum model approximation.[37] The MD simulations were done for *trans* and *cis* isomers of Cu(L-Val)$_2$ separately. Periodic boundary conditions were applied. One Cu(L-Val)$_2$ molecule was solvated in a rectangular box containing 3435 water molecules, and equilibrated for 500 ps. Four, eight, and 16 Cu(L-Val)$_2$ molecules were solvated in the same dimension cubic boxes containing 10316, 10264, and 10139 water molecules, respectively, and equilibrated for 500 ps. Productive MD phases were accomplished under constant temperature and pressure (298.15 K and 1 bar) using Berendsen T-coupling (τ_T = 0.1 ps) and Berendsen p-coupling (τ_p = 0.5 ps).[69] The time step was 1 fs. The water molecule's geometry was constrained by the SETTLE procedure,[70] whereas all Cu(L-Val)$_2$ degrees of freedom were relaxed during the MD simulations. A cutoff limit of 1.5 nm was applied for the calculations of Coulomb and Lennard-Jones 12−6 interactions. The cutoff distance for the short-range neighbor list was set to 1.0 nm. Additionally, two 50-ns MD simulations were performed for the 84Cu(L-Val)$_2$·84H$_2$O system at 298.15 and 370 K.

RESULTS AND DISCUSSION

X-ray Crystal and Molecular Structures. Compound *trans* Cu(L-Val)$_2$ crystallized in the triclinic *P*1 space group with one complex molecule per asymmetric unit. The Cu(II) cation is hexacoordinated, with the O11, N11, O21, and N21 atoms in the equatorial positions, and two carbonyl oxygen atoms O12^{i} and O22^{ii} of the neighboring molecules occupying the apical positions of a distorted bipyramid (Figure 1a, Table 2). Both chelate rings are significantly puckered (Table 2). Compound *cis* Cu(L-Val)$_2$·H$_2$O crystallized in the monoclinic *C*2 space group with one complex molecule per asymmetric unit. The Cu(II) cation is pentacoordinated, with a coordination geometry that conforms to a distorted square pyramid. The water molecule O31 atom occupies the apical position of the pyramid, and the O11, N11, O21, and N21 atoms occupy the four remaining square-base positions (Figure 1b, Table 2). Both chelate rings of the *cis* isomer are fairly planar (Table 2). In both complexes one chelate ring exhibits a δ-envelope and the other a λ-envelope absolute configuration. The *iso*-propyl moieties bonded to the λ- and δ-chelate envelopes are in the axial and equatorial positions, respectively. Both *iso*-propyl groups of the *cis* isomer are disordered.

The *trans* Cu(L-Val)$_2$ molecules self-assembled into a 1D coordination polymer by the Cu···O$_{carbonyl}$ coordinative bonds and by two N−H···O hydrogen bonds (Supporting Information, Figure S1a). The 1D polymers were connected into a molecular sheet via four N−H···O hydrogen bonds and two C−H···O interactions (Supporting Information, Figure S1b). The sheets stacked offset and were connected by dispersion forces into a 3D (graphite-like) structure. Moreover, the *iso*-propyl moieties are locked by two weak *intra*chain and two *inter*chain C−H···O interactions (Supporting Information, Figure S1). Such interactions are absent in the *cis*-isomer crystal phase. In the crystal phase of the *cis* compound, the Cu(L-Val)$_2$·H$_2$O building blocks formed two O−H···O hydrogen bonds with carbonyl oxygen atoms O12 and O22 of the neighboring molecules (Supporting Information, Figure S2). In this manner formed 2D molecular layers were further interlinked by four N−H···O hydrogen bonds. *Iso*-propyl moieties protruded from those layers, and as the sheets stacked offset because of the dispersion forces, a 3D porous structure was formed (Supporting Information, Figure S3). Although both crystal structures are layered, the *trans* compounds are packed denser than the *cis* ones. Less compact packing in the *cis* crystal phase

dx.doi.org/10.1021/ic102585f |*Inorg. Chem.* 2011, 50, 3632–3644

Table 2. Selected X-ray Crystal Bond Distances (Å) and Angles (deg) of *trans* Cu(L-Val)$_2$ and *cis* Cu(L-Val)$_2$·H$_2$O and Their Corresponding Values in the Minimum FFWa-SPCE Crystal Structures[a]

	X-ray		FFWa-SPCE		
				cis Cu(L-Val)$_2$·H$_2$O	
internal coordinate	*trans* Cu(L-Val)$_2$	*cis* Cu(L-Val)$_2$·H$_2$O[b]	*trans* Cu(L-Val)$_2$	ca1-ce1	ca2-ce1
		Bond Distances			
Cu−O11	1.934(2)	1.950(3)	1.918	1.920	1.920
Cu−O21	1.942(2)	1.930(3)	1.924	1.924	1.925
Cu−N11	1.987(3)	1.991(3)	1.991	1.993	1.994
Cu−N21	2.009(3)	2.005(4)	1.994	1.995	1.994
Cu−O31		2.360(2)		2.574	2.535
Cu−O12^{i}	2.617(2)		2.222		
Cu−O22^{ii}	2.779(2)		2.455		
		Valence Angles			
O11−Cu−O21	178.45(13)	90.43(11)	174.4	84.7	80.6
O11−Cu−N21	96.18(10)	162.99(15)	95.7	151.5	159.2
O21−Cu−N21	83.38(11)	84.22(15)	84.9	85.8	85.8
O11−Cu−N11	84.02(10)	83.84(11)	86.0	86.5	86.2
O21−Cu−N11	96.27(10)	171.89(15)	92.6	165.0	154.8
N11−Cu−N21	174.00(11)	99.65(17)	172.8	96.3	100.1
		Torsion Angles			
O11−C11−C12−N11	−27.9(3)	−14.7(3)	−23.1	−15.0	−22.5
O21−C21−C22−N21	41.3(3)	11.4(3)	41.8	19.5	17.9
C14−C13−C12−N11	−59.7(3)		−73.0		
C13−C12−N11−Cu	−91.42(19)		−97.7		
C14B−C13B−C12−N11		−75.2(1)			−78.6
C13B−C12−N11−Cu		−97.1(5)			−100.8
C14A−C13A−C12−N11		72.8(9)		63.1	
C13A−C12−N11−Cu		−118.7(7)		−110.9	
C24−C23−C22−N21	−53.7(2)	57.8(7)	−58.9	60.8	60.8
C23−C22−N21−Cu	−172.26(15)	−139.2(4)	−168.4	−152.1	−150.6
O21−N21−N11−O11	175.3(1)	7.1(1)	178.4	9.3	−3.4

[a] Symmetry codes: $i = 1 + x, y, z$; $ii = -1 + x, y, z$. [b] The disordered moieties include C13A, C14A, C13B, and C14B atoms.

may be influenced by disordered *iso*-propyl moieties. The hydrogen bond distances and angles for both crystal structures are listed in Supporting Information, Table S1.

Thermal Analysis, FTIR Spectra, and PXRD Patterns. TG curve of the *cis* Cu(L-Val)$_2$·H$_2$O sample taken from the bulk obtained by recrystallization shows two mass losses (Supporting Information, Figure S4a). First mass loss, from 30 to 220 °C, is caused by liberation of water molecules. Second mass loss, from 190 to 270 °C, is caused by partial sublimation and pyrolitic decomposition of the sample. In the similar temperature intervals there are strong endothermic signals in the DSC curves measured for the samples of *cis* Cu(L-Val)$_2$·H$_2$O, the product obtained by one-day thermal treatment of *cis* Cu(L-Val)$_2$·H$_2$O, and *trans* Cu(L-Val)$_2$ (Supporting Information, Figure S4b). The temperature of the DSC peak maximum, T_{max}, is the lowest for *cis* Cu(L-Val)$_2$·H$_2$O and the highest for *trans* Cu(L-Val)$_2$.

The FTIR spectra of *cis* Cu(L-Val)$_2$·H$_2$O and of the product obtained by the thermal treatment are very similar (Supporting Information, Figure S4c). However, in the latter one, in the region from 3200 to 3400 cm^{-1}, the broad band corresponding to the water molecule vibrations is reduced (because of the dehydration) revealing a very strong N−H vibrational band at 3297 cm^{-1}, broadened probably because of amino groups' involvement in hydrogen bonding.

Comparison of the experimental PXRD patterns with those simulated from the single-crystal data confirmed the identity of *cis* Cu(L-Val)$_2$·H$_2$O and *trans* Cu(L-Val)$_2$ powder samples (Supporting Information, Figure S4d). However, the PXRD pattern of the dehydration product obtained by the thermal treatment of *cis* Cu(L-Val)$_2$·H$_2$O does not fit the PXRD pattern either of *trans* Cu(L-Val)$_2$ or *cis* Cu(L-Val)$_2$·H$_2$O (Supporting Information, Figure S4d). Unfortunately, it is not yet possible to experimentally reveal the exact structure of that solid phase.

MM Reproduction of the X-ray Crystal and Molecular Structures. To test the ability of the FFWa-SPCE force field to reproduce the experimental crystal and molecular structures of *trans* Cu(L-Val)$_2$ and *cis* Cu(L-Val)$_2$·H$_2$O, the experimental crystallographic data were taken as the starting point for geometry optimization using the crystal simulator[65] of the Lyngby-CFF program. The superpositions of the X-ray and MM derived unit cells and packings are illustrated in Figures 2 and 3. Because the *cis*-isomer is disordered in the crystal structure, two

dx.doi.org/10.1021/ic102585f |*Inorg. Chem.* 2011, 50, 3632–3644

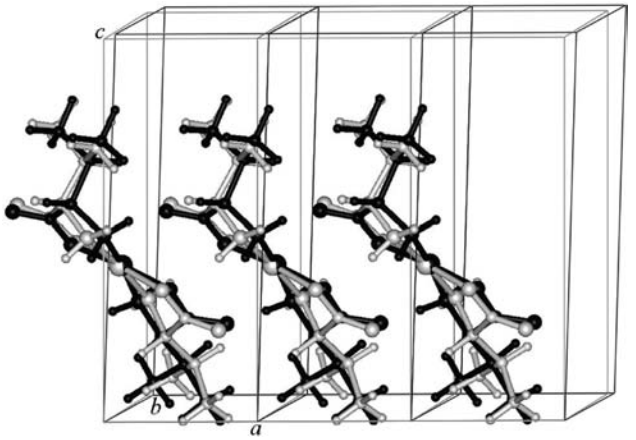

Figure 2. Superposition of the X-ray (light gray) and FFWa-SPCE crystal (black) unit cells and packing of *trans* Cu(L-Val)$_2$. FFWa-SPCE crystal unit cell dimensions: a = 4.911 Å, b = 5.411 Å, c = 12.417 Å, α = 75.3°, β = 88.5°, γ = 77.7°, V = 311.6 Å^3.

FFWa-SPCE crystal structures were calculated as if the two most populated conformers (the conformers were named ca2-ce1 and ca1-ce1, Table 2, Figure 3) were solely present in the crystal lattice. The efficacy of the experimental data reproduction is measured by the root-mean-square (rms) deviations and differences between the X-ray and FFWa-SPCE crystal internal coordinates and unit cell dimensions (Table 3).

The error values (Table 3) are within the ranges of the FFWa-SPCE reproduction errors obtained for previously studied anhydrous and aqua Cu(aa)$_2$ complexes,[37] except that the rms($\Delta\theta$) values of the ca2-ce1 and ca1-ce1 conformers are slightly higher (up to 1.5°) because of a more distorted copper(II) coordination polyhedron in the MM structures than in the experimental one (Table 2). Such result is acceptable because the real crystal structure organization composed of the two conformers cannot be built and simulated by the Lyngby-CFF crystal simulator. As FFWa-SPCE generally overestimates the Cu to axial O_{water} distances (by 0.2 Å on average),[37] the reproduction of the Cu to O31 distance (Table 2) is in accord with the FFWa-SPCE mean value of 2.65(15) Å calculated for earlier studied 11 aqua copper(II) amino acidates.[37]

In the MM *trans* Cu(L-Val)$_2$ unit cell, although the experimental position of the copper atom is well reproduced (Figure 2), the orientation of the chelate rings is slightly tilted in an opposite direction, and the molecules formed shorter N−H···$O_{carbonyl}$ and longer N−H···$O_{carboxyl}$ hydrogen bonds (Supporting Information, Table S2), and closer Cu···$O_{carbonyl}$ distances (Table 2) than in the X-ray crystal structure (Supporting Information, Table S1). Namely, one of several specific conditions used in the FFWa-SPCE parametrization procedure[37] was to reproduce the span of experimental intermolecular Cu···$O_{carbonyl}$ distances from 2.31 to 3.12 Å observed in 8 earlier studied Cu(aa)$_2$ complexes.[37] The FFWa-SPCE reproduced this relatively large distance span in the range from 2.38 to 2.88 Å.[37] The new MM simulation result reveals that FFWa-SPCE can yield Cu···$O_{carbonyl}$ even shorter than 2.38 Å in the case of such dense crystal packing like of the *trans* Cu(L-Val)$_2$ isomer, and with all unit cell dimensions and atomic coordinates allowed to be varied during the geometry optimization. However, this did not dramatically disturb the unit cell packing reproduction as the unit cell dimensions, and the

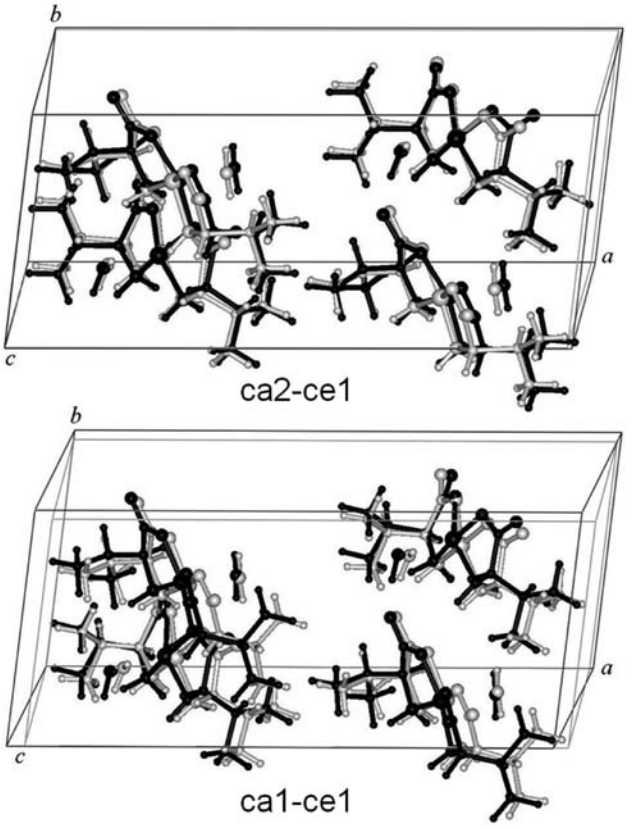

Figure 3. Superposition of the X-ray (light gray) and FFWa-SPCE crystal (black) unit cells and packing of *cis* Cu(L-Val)$_2$·H$_2$O. FFWa-SPCE crystal unit cell dimensions: a = 21.497 Å, b = 9.667 Å, c = 7.516 Å, β = 108.7°, V = 1479.7 Å^3 (ca2-ce1 conformer); a = 21.487 Å, b = 9.987 Å, c = 7.737 Å, β = 113.9°, V = 1517.6 Å^3 (ca1-ce1 conformer).

intramolecular internal coordinates (especially of the CuN_2O_2 coordination polyhedron, Table 2) were well reproduced (Table 3, Figure 2). Good match between the experimental and MM structures, illustrated in Figures 2 and 3, may confirm that in general FFWa-SPCE accurately reproduces the crystal lattice effects.

Conformational Analyses. The conformational analyses of *trans* and *cis* isomers of Cu(L-Val)$_2$ were performed in vacuo and in simulated crystal by MM calculations, and in aqueous solution by MD simulations to rationalize the influence of intermolecular interactions on the geometry changes and the energy distribution among the conformers. From the stereochemical and theoretical points of view, each chelate ring of Cu(L-Val)$_2$ molecule can have 6 conformations, that is, two conformations of the five-atom chelate ring having C^β in an axial position and C^β in an equatorial position (λ- and δ-envelope absolute configurations, respectively), and three conformations of the valine residue characterized by the torsion angle C^γ-C^β-C^α-N ≈ 60°, −60°, and 180°. The six chelate-ring conformations, whose combinations yield the total of 21 conformers with *trans*-configuration and 21 conformers with *cis*-configuration, are defined in Figure 4. The conformers were constructed from the experimental atomic coordinates. The experimentally occurring conformers are *trans* ta2-te2, and *cis* ca2-ce1 and ca1-ce1.

Conformational Analysis in Vacuo. The equilibrium vacuum geometries were calculated for the Cu(L-Val)$_2$ molecule alone, and for a system of the Cu(L-Val)$_2$ molecule interacting with one

dx.doi.org/10.1021/ic102585f |*Inorg. Chem.* 2011, 50, 3632–3644

Table 3. Root-Mean-Square, rms, Deviations and Differences, Δ, Calculated between the X-ray and FFWa-SPCE Crystal Internal Coordinates and Unit Cell Dimensions[a]

	internal coordinates			unit cell dimensions		
compound	rms(Δb)	rms($\Delta\theta$)	rms($\Delta\varphi$)	rms(Δa,Δb,Δc)	$\Delta\alpha$,$\Delta\beta$,$\Delta\gamma$	$100\Delta V/V_{exp}$
trans Cu(L-Val)$_2$	0.011	1.7	5.2	0.153	4.1, 1.3, 1.7	−2.8
cis Cu(L-Val)$_2$·H$_2$O[b]						
ca1-ce1	0.023	3.6	6.4	0.303	0.0, −5.0, 0.0	−5.5
ca2-ce1	0.021	4.7	6.5	0.110	0.0, 0.2, 0.0	−2.9

[a] Internal coordinates: bond lengths, b (in Å), valence angles, θ (in deg), torsion angles, φ (in deg). Hydrogen atoms were not taken into account. Unit cell dimensions: unit cell lengths, a, b, and c (in Å), unit cell angles, α, β, and γ (in deg), and volume, V. [b] Too short and too large experimental internal coordinates C12−C13A = 1.445(9) Å, C12−C13B = 1.674(12) Å, and C24−C23−C25A = 123.7(1)° of the disordered moieties were excluded from the comparisons.

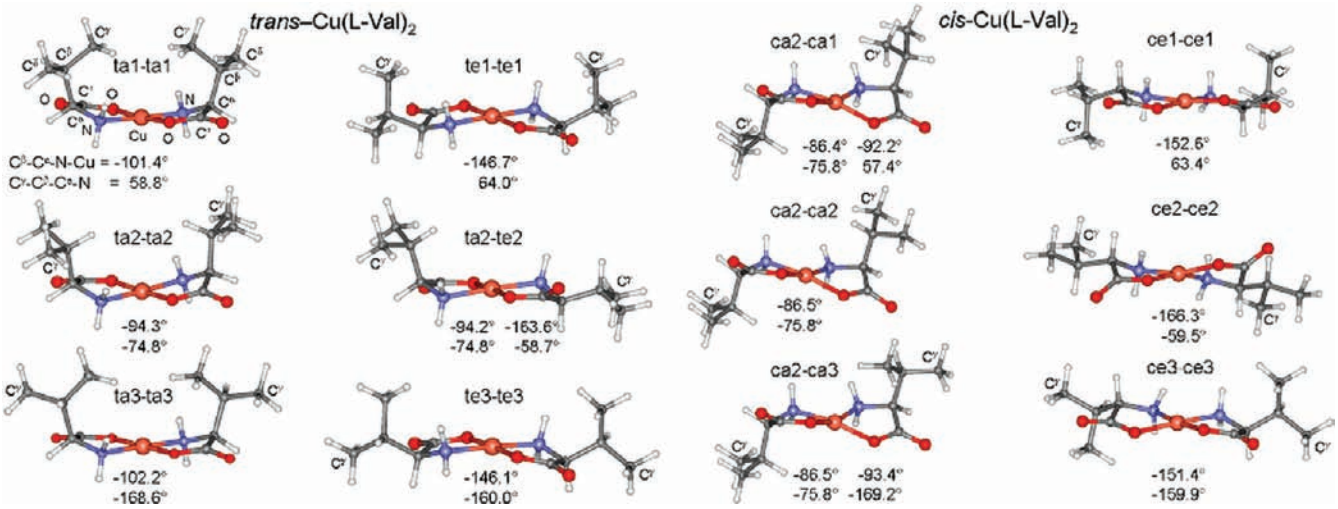

Figure 4. Definition of six chelate-ring conformations differentiated by the values of denoted torsion angles in selected 6 *trans* and 6 *cis* Cu(L-Val)$_2$ conformers.

water molecule, Cu(L-Val)$_2$·H$_2$O. Figure 5 presents the lowest V_{vacuum} values calculated for all constructed conformers. Generally, the V_{vacuum} values are significantly lower for the *trans*- than the *cis*-conformers. However, the presence of a water molecule in the system decreased the energy difference estimated between the most stable *cis* and *trans* conformers, ca2-ca3 and ta3-ta3, from 96 kJ mol^{-1} in the anhydrous system to 80 kJ mol^{-1} in the Cu(L-Val)$_2$·H$_2$O system. Moreover, the interactions between Cu(L-Val)$_2$ and H$_2$O enabled obtaining minimum structures of several *cis*-conformers which otherwise transformed to the corresponding *trans*-ones in the anhydrous system during the geometry optimization (Figure 5).

Conformational Analysis in Crystal. We used the atomic coordinates constructed for all possible 21 *trans* and 21 *cis* conformers, the experimental X-ray unit cell lengths and angles, the *C*2 and *P*1 space group symmetry operations for the aqua and anhydrous Cu(L-Val)$_2$, respectively, and the molecule orientation defined according to the experimental ones (detailed description is given in Supporting Information) as starting data for the energy minimization in simulated crystalline environment. Our intention in predicting the unit cell packing of different conformers has not been to search the global minimum in the crystal packing but to get an insight into the energy values of the *trans*- relative to the *cis*-conformers in the anhydrous and hydrated crystal structures. We assumed that during the geometry optimization each conformer would adopt an optimal orientation and form as close intermolecular interactions (i.e., N−H···O, O−H···O, and C−H···O bonding, aliphatic-aliphatic close contacts, and axial Cu-to-O coordinative bonding) as possible with the surrounding molecules.

Figure 5 shows the lowest of the estimated $V_{in\text{-}crystal}$ and $V_{intermolecular}$ values among all attained conformers' packings. In the anhydrous crystal, the experimentally determined ta2-te2 conformer (Figure 2) has the lowest $V_{in\text{-}crystal}$ energy (by 37 kJ mol^{-1} lower than for the lowest anhydrous *cis* minimum ca3-ca3). In the hydrated system, the ca2-ce1 and ce1-ca1 conformers observed in the experimental crystal (Figure 3) have the lowest $V_{intermolecular}$ but not the $V_{in\text{-}crystal}$ energies. The result may be attributed to the inability to model two conformers in the same unit cell, to the force field's possible imperfections, or to some specific reasons occurring during the crystallization process. In the hydrated crystal, the lowest $V_{in\text{-}crystal}$ value (by 40 kJ mol^{-1} lower than for ca2-ce1) was calculated for the ca2-ca3 and ta3-te2 conformers. In their minimum unit cell packings, the water molecule was displaced from the copper(II) by forming O−H···O$_{carboxylato}$ hydrogen bonds, and an intermolecular Cu···O$_{carbonyl}$ bond of 2.6 Å (ta3-te2) and 2.7 Å (ca2-ca3) was formed.

The crystal structure predictions show that generally the conformations with C$^{\beta}$ atoms in the axial−equatorial positions

dx.doi.org/10.1021/ic102585f |*Inorg. Chem.* 2011, 50, 3632–3644

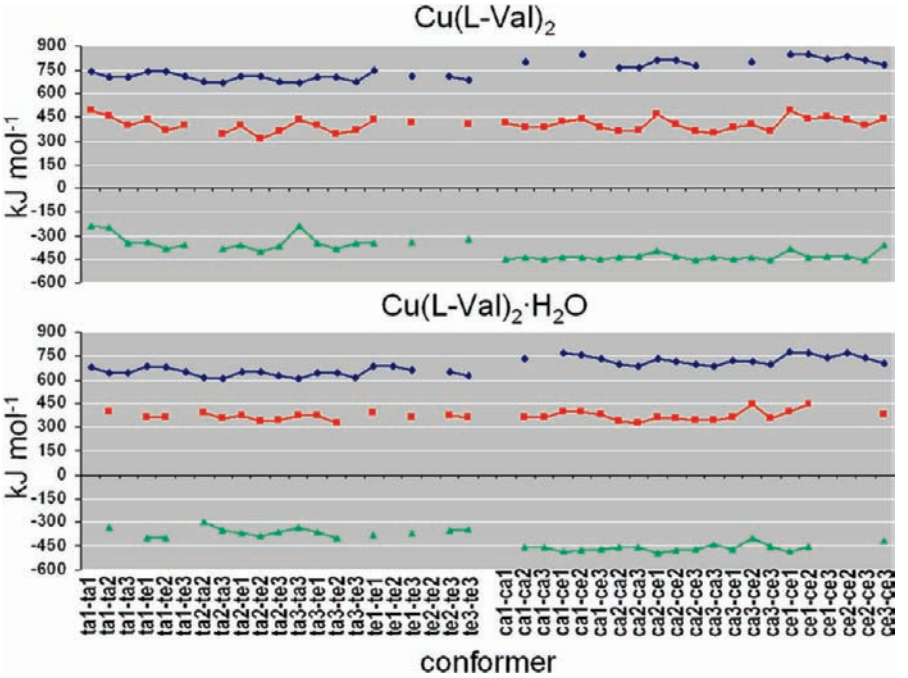

Figure 5. FFWa-SPCE minimum energy values estimated for 42 possible conformers of the Cu(L-Val)$_2$ and Cu(L-Val)$_2$·H$_2$O systems in the gas phase, V_{vacuum} (blue), and in simulated crystal packing, $V_{in\text{-}crystal}$ (red) and $V_{intermolecular}$ (green). An empty space means that the corresponding starting conformer changed to another conformer during the geometry optimization.

are better suited for the crystal packing, and that the *cis*-conformers have lower $V_{intermolecular}$ values than the *trans*-ones (Figure 5). Generally, the lowest-energy minima of *trans*- and *cis*-conformers had lower and higher $V_{in\text{-}crystal}$ values, respectively, in the anhydrous than aqua Cu(L-Val)$_2$ crystals, in accord with the experimental crystallization outcome. A reason that a *cis*-conformer did not crystallize as an anhydrous solid-state structure might be the insufficient $V_{intermolecular}$ to overcome the substantial intramolecular V_{strain} energy difference between the *cis* and *trans* conformers. However, the unit cell packing predictions suggest that the water molecules are required in the crystal lattice to attain lower in-crystal potential energy of the *cis*- relative to the *trans*-isomer, and thus enable the crystallization of the *cis*-isomer.

Conformational Analysis in Aqueous Solution. To explore further the influence of intermolecular interactions between the Cu(L-Val)$_2$ and water molecules on the geometry changes and the energy distribution among the conformers, the 20-ns MD simulations of the Cu(L-Val)$_2$·3435H$_2$O system at 298.15 K were performed. The starting *trans* and *cis* conformers were a1-a1, e2-e2, a3-a3, having the same valinato-residue conformation in both chelate rings, and a2-e1, having mixed different *iso*-propyl conformations. The e2-e2 conformer changed very fast to the a2-a2 one. For other conformers, the interchange between the conformations with C^{β} in axial and equatorial positions was observed, whereas the *iso*-propyl conformations remained unchanged. The distribution functions for the C^{β}-C^{α}-N-Cu angles calculated from the 20-ns MD data suggested the most prevailing conformers of the studied systems (Supporting Information, Table S3).

In line with the MD results obtained for the solvated *cis* and *trans* Cu(Gly)$_2$ systems,[37] during the 20-ns MD simulations a transition between the *cis* and *trans* Cu(L-Val)$_2$ configurations was not obtained,[71] and the average MD total energies of *cis* and *trans* Cu(L-Val)$_2$·3435H$_2$O systems (Supporting Information, Table S3) are almost the same for the same conformers. The solvated *trans* and *cis* a2-a2 systems had the lowest average total energy, the *cis* e1-e1 and e1-a1 conformers (followed by *cis* a2-e1) formed the most favorable intermolecular interactions with water molecules. Like in vacuo, the resulting average energy of the mixed a2-e1 conformer system can be considered as a half of the sum of average energies of the a2-a2 and e1-e1 conformers. Because the differences between the MD average energies among the studied conformers (up to 57 kJ mol^{-1}, Supporting Information, Table S3) are much lower than the energy rms deviations (the lowest rms deviation amounts to 243 kJ mol^{-1}, Supporting Information, Table S3), we may conclude that the *trans* and *cis* conformers having all possible *iso*-propyl conformations can be present in aqueous solution at room temperature.

MD Simulations of Self-Association of Cu(L-Val)$_2$ Molecules in Aqueous Solution at 298.15 K. The MD calculations were also applied for the systems of 4, 8, and 16 solvated Cu(L-Val)$_2$ molecules in water medium at 298.15 K to understand the self-association of the complexes in solution. The calculations were encouraged by the MD self-association modeling of 4 solvated *trans* and *cis* Cu(Gly)$_2$ molecules into a crystallization nucleus, which suggested faster aggregation of the *cis*- than *trans*-isomers,[37] confirming the experimental evidence[12,13] that *cis* Cu(Gly)$_2$·H$_2$O crystallized from aqueous solution. The systems with 4, 8, and 16 Cu(L-Val)$_2$ complexes solvated in the same-dimension cubic boxes corresponded to a very dilute solution, a dilute solution (related to the experimental system with starting 0.125 g of Cu(L-Val)$_2$ powder dissolved in 10 mL of water), and a saturated solution, respectively.[72] Two MD trajectories were collected for each of the 4Cu(L-Val)$_2$·10316H$_2$O, 8Cu(L-Val)$_2$·10264H$_2$O, and 16Cu(L-Val)$_2$·10139H$_2$O systems containing either *trans* or *cis* Cu(L-Val)$_2$ isomers during 50 ns, 40 ns, and 27980 ps, respectively. The ta2-ta2 and ce1-ce1 conformers were chosen as the starting conformations having the copper atoms in

dx.doi.org/10.1021/ic102585f |*Inorg. Chem.* 2011, 50, 3632–3644

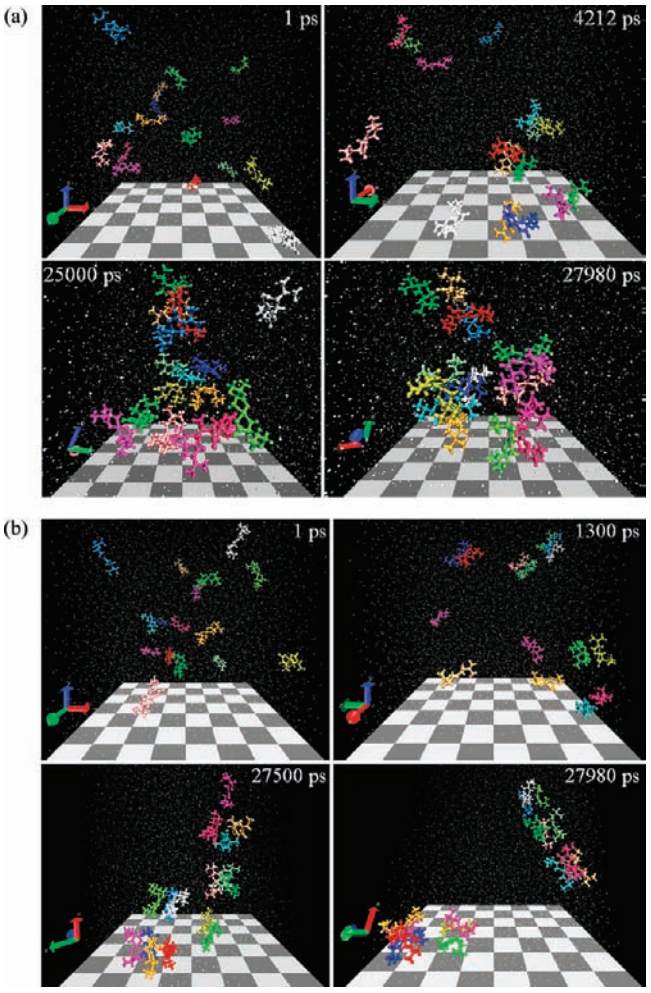

Figure 6. System of $16Cu(L\text{-}Val)_2 \cdot 10139H_2O$ depicted at indicated times in MD simulations: (a) 16 *trans* conformers with $C^{\gamma}\text{-}C^{\beta}\text{-}C^{\alpha}\text{-}N \approx -60°$ and (b) 16 *cis* conformers with $C^{\gamma}\text{-}C^{\beta}\text{-}C^{\alpha}\text{-}N \approx 60°$. Water molecules' oxygen atoms are in white. The figure was prepared using VMD.[73]

the same initial positions in the corresponding simulation boxes. During the simulations neither a change in the valinato side-chain conformations nor *cis-trans* isomerization was observed. After some time, the $Cu(L\text{-}Val)_2$ complexes started to aggregate. The aggregation times are given in the Supporting Information, Table S4. All combinations with C^{β}-axial and C^{β}-equatorial of the same *iso*-propyl conformations were identified in the aggregations.

In most cases, the monomers aggregated to the oligomers by forming $Cu\cdots O_{carboxylato}$ close contacts. Self-assembly could also proceed by $N-H\cdots O_{carboxylato}$ hydrogen bonding. Such case is a dimer−dimer binding into a tetramer, and then into a sextamer in the 16 *trans* $Cu(L\text{-}Val)_2$ system (sextamer2, Supporting Information, Table S4). Also, two dimers attached to each other by $N-H\cdots O_{carboxylato}$ bonds, and after that the complexes reoriented to form the $Cu\cdots O_{carboxylato}$ bonding in the 16 *cis* $Cu(L\text{-}Val)_2$ system (tetramer1, Supporting Information, Table S4). A monomer bound with a trimer by $N-H\cdots O_{carboxylato}$ bonding in the 8 *cis* $Cu(L\text{-}Val)_2$ system (tetramer, Supporting Information, Table S4). During the 40-ns MD simulations of the $8Cu(L\text{-}Val)_2 \cdot 10264H_2O$ systems, the *trans*-complexes aggregated to one tetramer and two dimers, while the *cis*-conformers formed a trimer-to-tetramer aggregation bound via a water molecules' layer by relatively weak $C-H\cdots O_{water}$ bonds (i.e., water-mediated interactions between the oligomers), and moved together through the water medium.

More information and details on possible formation of a crystallization nucleus were obtained from modeling of the systems containing 16 solvated complexes (Figure 6). At the end of 27980-ps MD simulations of the $16Cu(L\text{-}Val)_2 \cdot 10139H_2O$ systems, the *trans*-conformers formed a tetramer and two chain-like sextamer structures assembled by close van der Waals aliphatic-aliphatic interactions and via $C-H\cdots O_{water}$ interactions (Figure 6a). Differently, the *cis*-conformers self-associated into two layered aggregations composed of three trimers, and a dimer and a tetramer bound via $C-H\cdots O_{water}$ interactions (Figure 6b, Supporting Information, Table S4). The first water-mediated aggregations formed around 4400 and 7500 ps in the 16 *cis*- and 16 *trans*-isomer systems, respectively. Predicted different *trans*- and *cis*-isomer aggregation patterns (Figure 6) are in line with the experimental X-ray crystal structure organizations having the *trans*- and *cis*-isomers assembled into 1D chains and 2D sheets, respectively.

The MD simulations suggest that first the relatively strong $Cu\cdots O_{carboxylato}$ and $N-H\cdots O_{carboxylato}$ noncovalent bonds, and then the relatively weak water-mediated interactions between the formed aggregations could be the governing factors for the kinetic effects. The $Cu(L\text{-}Val)_2$ conformations can also influence the self-assembly as the aliphatic-aliphatic interactions certainly take part in bringing $Cu(L\text{-}Val)_2$ molecules together and fixing the oligomers into energetically favorable orientations thus allowing growth of the crystal nuclei. Generally, the dimers were formed faster by the *cis*- than *trans*- conformers (Supporting Information, Table S4). However, the *trans*-conformers aggregated faster than the *cis*-ones into a tetramer in the $4Cu(L\text{-}Val)_2$ systems (Supporting Information, Table S4), and into the $16Cu(L\text{-}Val)_2$ conglomerate (Figure 6). In contrast, the MD simulations of the $8Cu(L\text{-}Val)_2 \cdot 10264H_2O$ systems yielded faster aggregation of the *cis*- than *trans*- conformers (Supporting Information, Table S4). If we assume that modeling the self-assembly of *trans* and *cis* $Cu(L\text{-}Val)_2$ molecules in the $8Cu(L\text{-}Val)_2 \cdot 10264H_2O$ systems may represent the real event of dissolving $Cu(L\text{-}Val)_2$ powder containing prevailingly *trans*- or *cis*-conformers in water, the MD simulations suggest that some oligomers can be formed by both *trans*- and *cis*-isomers in the first 40 ns after the dissolvation. If so, these *trans*- and *cis*-oligomers formed quickly just upon the dissolvation (and before the *cis−trans* isomerization in monomers can take place and result in oligomers formed by both *cis*- and *trans*-isomers) may be the key factor that steers the nucleation and crystallization process toward either *cis* or *trans* crystal phase.

The average MD total energy values of the systems with 4, 8, and 16 solvated $Cu(L\text{-}Val)_2$ complexes being monomers as well as oligomers are lower for the *trans*- than the *cis*-systems (Supporting Information, Table S5). However, the MD predictions on the aggregation times in the three studied systems (Supporting Information, Table S4) are not straightforward enough to suggest which of the isomers aggregates faster. Anyway, by considering the calculations of the relative stabilities, and the experimental result that the hydrated *cis*-isomer is the product of both the synthesis and the subsequent recrystallization, it is possible to conclude that the *cis* hydrated solid-state structure of $Cu(L\text{-}Val)_2$ should be a kinetic product.

dx.doi.org/10.1021/ic102585f |*Inorg. Chem.* 2011, 50, 3632–3644

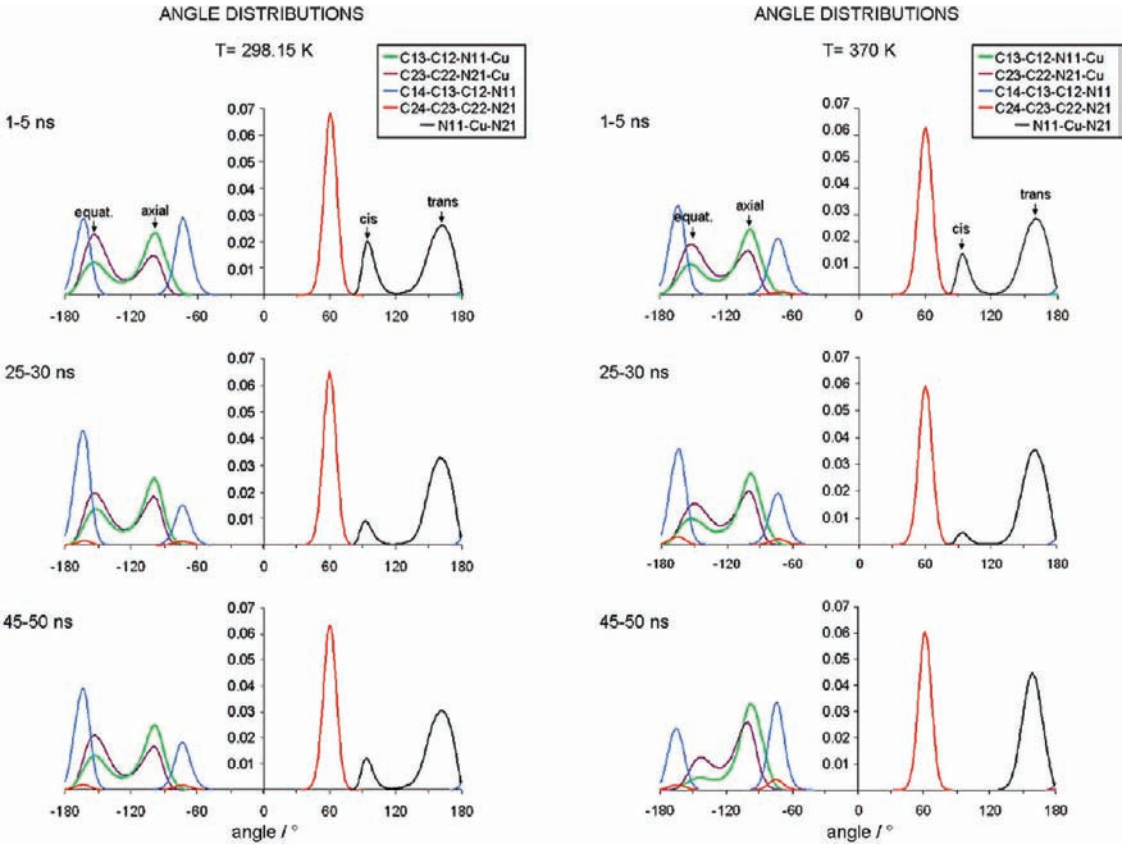

Figure 7. Angle distribution functions estimated from the data collected in indicated periods of the 50-ns MD simulations of the $84Cu(L\text{-}Val)_2 \cdot 84H_2O$ system. The atom labels are defined in Figure 1.

Fifty-Nanosecond MD Simulations of the $84Cu(L\text{-}Val)_2 \cdot 84H_2O$ System at 298.15 and 370 K. In an attempt to understand what factors influence different behavior of the initially synthesized and experimentally heated $Cu(L\text{-}Val)_2$ powder samples, we performed the MD simulations of the $84Cu(L\text{-}Val)_2 \cdot 84H_2O$ system (as a crude approximation of the polycrystalline system) at room temperature and 370 K. Our hypothesis was that one-day heating of the *cis* $Cu(L\text{-}Val)_2 \cdot H_2O$ powder sample could bring enough energy to the system to enable either the transformation of *cis*-to-*trans*-configuration or/and a conformational change. We assumed two scenarios as possible: (1) a complete *cis*-to-*trans* isomerization by the heating process; then by dissolving the thermally treated compound the prevalence of *trans*-conformers in aqueous solution would steer the crystal growth process toward a *trans*-isomer; or/and (2) a conformational change by the rotation around the C^{β}-C^{α} bond, from the e1/a1 conformations (C^{γ}-C^{β}-C^{α}-N $\approx 60°$) to other conformations (that generally have lower intramolecular energy values, Figure 5); such event would eliminate the possibility for the ca1-ce1 and ca2-ce1 conformers, having the most favorable intermolecular interactions with water molecules (Supporting Information, Table S3) to crystallize from aqueous solution.

For the $84Cu(L\text{-}Val)_2 \cdot 84H_2O$ system, the experimental atomic coordinates of the ca2-ce1 conformers and their axially placed water molecules were taken as the starting data, and the system was confined in a cubic box. After the energy minimization (to get rid of bad contacts), and 500 ps of equilibration phase, we followed the system reorganization during 50 ns of MD simulations. Different behavior of the system examined at 298.15 and 370 K was attained (Figure 7).

During the 50-ns simulations, at 370 K all conformers gradually transformed from the *cis*- to the *trans*-isomer (Figure 7). Although at 298.15 K the *trans*-conformers were more numerous than the *cis*-ones, which may contradict the experimental evidence, the transition from *trans*- to *cis*-configuration was also happening, and the number of *cis*-conformers increased during the last 5 ns of the simulation compared to the 25−30 ns simulation period (Figure 7). During the simulations, the C24-C23-C22-N21 angle (Figure 1) changed subsequently from the initial approximate 60° to about −60°, and then to 180° in altogether 4 and 9 conformers at 298.15 and 370 K, respectively. For the simulation period of 45−50 ns (Figure 7), at 370 K the number of conformations with C^{β} in the axial position in both chelate rings increased, whereas at 298.15 K the C^{β} atoms in most conformers retained the initial experimental axial−equatorial positions.

At the end of the 50-ns MD simulations, the prevailing conformers were *trans* and *cis* a3-e1 and a2-e1 at 298.15 K, and mostly ta2-ta1, then ta3-ta1, ta3-te1, and ta2-te1 at 370 K. At 370 K, the $Cu(L\text{-}Val)_2$ molecules formed an ordered chain-like structure via $Cu\cdots O_{carboxyl} \approx 2.5$ Å bonding (whose interaction contribution may be overestimated like in the simulation of the anhydrous *trans* $Cu(L\text{-}Val)_2$ crystal structure by FFWa-SPCE, which yielded too short $Cu\cdots O_{carbonyl}$ distances); the Cu to Cu close distances were around 4 Å, and the water molecules were between the chains. Such organization represents an easy pathway for the water molecules to leave the system by evaporation. In addition, the radial distribution function calculated for the distances between the Cu and O_{water} atoms revealed that most

dx.doi.org/10.1021/ic102585f |*Inorg. Chem.* 2011, 50, 3632–3644

water molecules were part of the Cu(II) first coordination sphere at 298.15 K. However, no water molecules were in the Cu(II) first coordination sphere at 370 K. These predictions are in accord with the experimental thermoanalytical, PXRD, and FTIR results (Supporting Information, Figure S4), that the structures of the initially synthesized and heated powder samples differ.

To summarize, the MD simulations of the complex "powder" predict that the change from *cis*- to *trans*-configuration can occur more readily than the change of the e1/a1 conformation. The simulations predict also frequent interchangeability between the a2/e2 and a3/e3 conformers (i.e., C^{γ}-C^{β}-C^{α}-N $\approx -60°$ and 180°, Figure 7) at both temperatures. From the sterochemical point of view it can be seen that this interchangeability can happen easier than between the e1/a1 and other conformers because of pronounced steric hindrance upon the rotation around the C^{β}-C^{α} bond in the latter case. Even though, the MD simulations show that these conformational changes (obstructed in aqueous solution by the intermolecular interactions between the complex and the water molecules) can happen quicker at 370 K than at 298.15 K. The MD simulations as well as the recrystallization from aqueous solution of the thermally treated powder suggest that the *trans*-isomer should be a thermodynamic product.

CONCLUSIONS

The application of the FFWa-SPCE force field for the MM and MD simulations in vacuo, in the solid state, and in aqueous solutions proved useful to understand the physicochemical mechanism going on at the nanoscale level, governing the formation of nucleus of crystallization, and crystallization process of either *cis*- or *trans*-isomer of Cu(L-Val)$_2$ from aqueous solution.

The estimated conformational analyses yield that although in vacuo the *cis*-conformers are predicted to be less stable than the *trans*-ones, more favorable intermolecular interactions of the *cis*- than the *trans*-conformers with the water molecules enable the existence of both isomers in aqueous solution, in accord with the EPR results.[31−33] The crystal structure predictions show that the 1:1 combination of *cis* Cu(L-Val)$_2$ and H_2O in an asymmetric unit stabilizes the *cis*-isomer crystal packing with respect to the corresponding *trans*-one. The most favorable intermolecular interactions that the *cis* conformers ca1-ce1 and ca2-ce1 form in the hydrated crystal structure and with water molecules in aqueous solution should explain their prevalence in the experimental crystal structure upon evaporation from aqueous solution.

The 27980-ps MD modeling of the self-association of 16 Cu(L-Val)$_2$ molecules in aqueous solution predicted different *trans*- and *cis*-isomer aggregation patterns, in line with their X-ray crystal structure organizations. The crystal nucleus formation was predicted to start by monomers' aggregation into oligomers by Cu···$O_{carboxylato}$ and/or N−H···$O_{carboxylato}$ noncovalent bonds. After that, the oligomers subsequently aggregated via the water molecules and diffused together until they eventually acquired right positions to form intermolecular aliphatic-aliphatic interactions, and/or N−H···$O_{carboxylato}$ hydrogen bonding that resembled the noncovalent bonding in experimental crystal structures, mimicking the aggregation growth to possible crystal structures.

The 50-ns MD simulations of the approximated polycrystalline system accomplished at 298.15 and 370 K predicted complete *cis*-to-*trans* isomerization at the higher temperature. If so, by considering the MD nucleation simulation result that both *cis*- and *trans*-conformers can self-assemble to oligomers just upon the dissolvation, it seems reasonable to assume that by dissolving the "heated" powder in water most of the conformers would retain the energetically preferred *trans*-configuration upon aggregation (even if the possibility of the *trans-cis* isomerization in solution cannot be neglected at the time scale of millisecond or longer). Under conditions close to the solid phase formation when the conformational changes can happen easier than in aqueous solution, the crystal structure predictions confirm that the *trans*-isomer would prefer anhydrous solid-state structure, and that the experimentally observed ta2-te2 conformer has the lowest in-crystal potential energy. Although the MM and MD results successfully assisted the experimental data to establish the relationship between the structural changes affected by the heating and the crystallization of specific geometry isomer, their full confirmation requires additional experimental substantiation. The sound simulation results encourage similar molecular modeling studies to evaluate kinetic and thermodynamic effects of bioinorganic systems.

ASSOCIATED CONTENT

Supporting Information. X-ray crystallographic informational files (CIF) are available for compounds *cis* Cu(L-Val)$_2$·H_2O and *trans* Cu(L-Val)$_2$. Illustrations of the hydrogen-bonding pattern in *trans* Cu(L-Val)$_2$ (Figure S1) and *cis* Cu(L-Val)$_2$·H_2O (Figure S2), porous crystal packing of *cis* Cu(L-Val)$_2$·H_2O (Figure S3), and TG and DSC thermograms, FTIR spectra, PDXR patterns measured for *cis* Cu(L-Val)$_2$·H_2O, *trans* Cu(L-Val)$_2$ and the product obtained by thermal treatment of *cis* Cu(L-Val)$_2$·H_2O, and simulated PDXR patterns of *cis* Cu(L-Val)$_2$·H_2O and *trans* Cu(L-Val)$_2$ (Figure S4). Listing of selected hydrogen-bond distances and angles for the X-ray (Table S1) and FFWa-SPCE crystal structures (Table S2) of *trans* Cu(L-Val)$_2$ and *cis* Cu(L-Val)$_2$·H_2O; MD average values and rms deviations of energy contributions calculated from the values attained during 20-ns MD simulations at 298.15 K for several conformers of *trans* and *cis* Cu(L-Val)$_2$·3435H_2O systems (Table S3), as well as from the data acquired during the first and the last 5 ns of productive MD simulations for the 4Cu(L-Val)$_2$·10316H_2O, 8Cu(L-Val)$_2$·10264H_2O, and 16Cu(L-Val)$_2$·10139H_2O systems (Table S5); aggregation times of 4, 8, and 16 solvated Cu(L-Val)$_2$ molecules during the MD simulations (Table S4). Details on the construction of initial data for energy minimization in simulated crystal surroundings. The 3D rendering for FFWa-SPCE crystal structures of Figures 2 and 3 in pdb format. This material is available free of charge via the Internet at http://pubs.acs.org.

AUTHOR INFORMATION

Corresponding Author
*E-mail: jasmina.sabolovic@imi.hr.

ACKNOWLEDGMENT

This work was supported by the Croatian Ministry of Science, Education and Sports (Project Grants 022-0222148-2822 and 119-1193079-1084). We thank Professor Dubravka

Matković-Čalogović and Dr Sanja Tomić for critical reading and editing of the manuscript.

REFERENCES

(1) Freeman, H. C. *Adv. Protein Chem.* **1967**, *22*, 257–424.

(2) Bruno, I. J.; Cole, J. C.; Edgington, P. R.; Kessler, M.; Macrae, C. F.; McCabe, P.; Pearson, J.; Taylor, R. *Acta Crystallogr.* **2002**, *B58*, 389–397.

(3) The crystal structures and the Cambridge Crystallographic Data Centre (CCDC) reference codes known for $Cu(aa)_2$ complexes: *trans* isomers of copper(II) complexes with alanine (CUALTE02, CUALTE01, CUALTE), asparagine (LASPCU01, LASPCU), leucine (LLEUCU), threonine (LTRECU01, LTRECU), phenylalanine (PEALCU10), methionine (TBLMCU), tyrosine (TYRSCU11, TYRSCU10), proline (XIDSEI) and glutamine (XUKXAC01, XUKXAC); *cis* isomers of copper(II) complexes with glycine (CUGLYM02, CUGLYM01, CUGLYM), alanine (CIYQAC01, CIYQAC, CALNCU10), isoleucine (ALEUCU01, ALEUCU), valine (CUNDAQ01, CUNDAQ), serine (LSERCU10 and NAYVEP) and phenylalanine (CEBREG).

(4) Kaitner, B.; Kamenar, B.; Paulić, N.; Raos, N.; Simeon, Vl. *J. Coord. Chem.* **1987**, *15*, 373–381.

(5) Kaitner, B.; Meštrović, E.; Paulić, N.; Sabolović, J.; Raos, N. *J. Coord. Chem.* **1995**, *36*, 117–124.

(6) Kaitner, B.; Paulić, N.; Raos, N. *J. Coord. Chem.* **1991**, *22*, 269–279.

(7) Kaitner, B.; Ferguson, G.; Paulić, N.; Raos, N. *J. Coord. Chem.* **1992**, *26*, 105–115.

(8) Kaitner, B.; Paulić, N.; Pavlović, G.; Sabolović, J. *Polyhedron* **1999**, *18*, 2301–2311.

(9) Coville, N. J.; Levendis, D. C. *Eur. J. Inorg. Chem.* **2002**, 3067–3078.

(10) Herlinger, A. W.; Wenhold, S. L.; Long, T. V., II *J. Am. Chem. Soc.* **1970**, *92*, 6474–6481.

(11) Yasui, T.; Shimura, Y. *Bull. Chem. Soc. Jpn.* **1966**, *39*, 604–608.

(12) Freeman, H. C.; Snow, M. R.; Nitta, I.; Tomita, K. *Acta Crystallogr.* **1964**, *17*, 1463–1469.

(13) Casari, B. M.; Mahmoudkhani, A. H.; Langer, V. *Acta Crystallogr.* **2004**, *Sect. E60*, m1949–m1951.

(14) Judaš. N. Ph.D. Thesis, University of Zagreb, Zagreb, Croatia, 2004.

(15) Hitchman, M. A.; Kwan, L.; Engelhardt, L. M.; White, A. H. *J. Chem. Soc., Dalton Trans.* **1987**, 457–465.

(16) Moussa, S. M.; Fenton, R. R.; Kennedy, B. J.; Piltz, R. O. *Inorg. Chim. Acta* **1999**, *288*, 29–34.

(17) Judaš, N.; Raos., N. *Inorg. Chem.* **2006**, *45*, 4892–4894.

(18) Gillard, R. D.; Mason, R.; Payne, N. C.; Robertson, G. B. *J. Chem. Soc. (A)* **1969**, 1864–1871.

(19) There are three reported X-ray crystal structures of *cis* $Cu(L\text{-}Val)_2 \cdot H_2O$, all of low quality and correspondingly with no H-atoms coordinates having the CCDC reference codes: CUNDAQ (ref 20; *R*-factor = 8.9%); CUNDAQ01 (ref 21; *R*-factor = 12%; also no valinato side chain atoms coordinates provided; this paper reports also the single crystal EPR spectra of *cis* $Cu(L\text{-}Val)_2 \cdot H_2O$); CUNDAQ02 (ref 22; *R*-factor = 5.58%, atomic coordinates are not available).

(20) Kangjing, Z.; Jinling, H.; Jianmin, L.; Yongfeng, Z.; Ping, Z. *Jiegou Huaxue (Chin.) (Chin. J. Struct. Chem.)* **1984**, *3*, 155.

(21) Steren, C. A.; Calvo, R.; Castellano, E. E.; Fabiane, M. S.; Piro, O. E. *Phys. B (Amsterdam)* **1990**, *164*, 323–330.

(22) Weng, J.; Liu, C.; Zheng, X.; Sun, C. *Fujian Shifan Dax. Xue., Zir. Kex. (Chin.) (J. Fujian Normal Univ. (Nat. Sci.))* **2002**, *18*, 50.

(23) Delf, B. W.; Gillard, R. D.; O'Brien, P. *J. Chem. Soc., Dalton Trans.* **1979**, 1301–1305.

(24) Xin, X.-Q.; Zheng, L.-M. *J. Solid State Chem.* **1993**, *106*, 451–460.

(25) Yoshikuni, T.; Tsuchiya, R.; Uehara, A.; Kyuno, E. *Bull. Chem. Soc. Jpn.* **1977**, *50*, 883–885.

(26) Tsuchiya, R.; Uehara, A.; Muramtsu, Y. *Bull. Chem. Soc. Jpn.* **1982**, *55*, 3770–3772.

(27) Fushimi, M.; Suzuki, M.; Uehara, A. *Bull. Chem. Soc. Jpn.* **1988**, *61*, 1809–1811.

(28) Sillen, L. G.; Martell, A. E. *Stability Constants of Metal Ion Complexes; Organic Ligands*; Chemical Society: London, 1964.

(29) Martell., A. E.; Smith, R. M. *Amino Acids. Critical Stability Constants*; Plenum Press: New York, 1974; Vol. 1.

(30) Dogan, A.; Köseoğlu, F.; Kiliç, E. *Anal. Biochem.* **2001**, *295*, 237–239.

(31) Goodman, B. A.; McPhail, D. B. *J. Chem. Soc., Dalton Trans.* **1985**, 1717–1718.

(32) Goodman, B. A.; McPhail, D. B.; Powell, H. K. J. *J. Chem. Soc., Dalton Trans.* **1981**, 822–827.

(33) Noethig-Laslo, V.; Paulić, N. *J. Chem. Soc., Dalton Trans.* **1992**, 2045–2047.

(34) Pezzato, M.; Della Lunga, G.; Baratto, M. C.; Pogni, R.; Basosi, R. *Magn. Reson. Chem.* **2007**, *45*, 846–849.

(35) DiDonato, M.; Sarkar, B. *Biochem. Biophys. Acta* **1997**, *1360*, 3–16.

(36) Tautermann, C. S.; Sabolović, J.; Voegele, A. F.; Liedl, K. R. *J. Phys. Chem. B* **2004**, *108*, 2098–2102.

(37) Sabolović, J.; Gomzi, V. *J. Chem. Theory Comput.* **2009**, *5*, 1940–1954.

(38) Sabolović, J. *AIP Conf. Proc.* **2009**, *1102*, 193–199.

(39) Neuberg, C.; Lustig, H.; Mandl, I. *Arch. Biochem. Biophys.* **1950**, *26*, 77–84.

(40) *Xcalibur CCD system, CRYSALIS Software system*, version 1.170; Oxford Diffraction Ltd.: Oxford, U.K., 2003.

(41) Sheldrick, G. M. *SHELXS97, Program for the Solution of Crystal Structures*; University of Göttingen: Göttingen, Germany, 1997.

(42) Sheldrick, G. M. *Acta Crystallogr.* **2008**, *A64*, 112–122.

(43) Farrugia, L. J. *J. Appl. Crystallogr.* **1999**, *32*, 837–838.

(44) Farrugia, L. J. *J. Appl. Crystallogr.* **1997**, *30*, 565.

(45) Macrae, C. F.; Edgington, P. R.; McCabe, P.; Pidcock, E.; Shields, G. P.; Taylor, R.; Towler, M.; van de Streek, J. *J. Appl. Crystallogr.* **2006**, *39*, 453–457.

(46) Valadon, P. *RasTop*, version 2.0.3.; La Jolla, CA, 2004; available at www.geneinfinity.org/rastop/

(47) *POV-Ray*; Persistence of Vision TM Raytracer, Pty. Ltd.: Williamstown, Australia, 2004.

(48) *X'Pert Organizer*, version 1.3e; Philips Analytical B. V.: Almelo, The Netherlands, 2001.

(49) *OPUS 4.0*; Brucker Optik GmbH: Ettlingen, Germany, 2003.

(50) Sabolović, J.; Mrak., Ž.; Koštrun, S.; Janeković, A. *Inorg. Chem.* **2004**, *43*, 8479–8489.

(51) Niketić, S. R.; Rasmussen, Kj. *The Consistent Force Field: A Documentation; Lectures Notes in Chemistry*; Springer-Verlag: Berlin, Heidelberg, New York, 1977; Vol. 3.

(52) Rasmussen, Kj. *Potential Energy Functions in Conformational Analysis; Lectures Notes in Chemistry*; Springer-Verlag: Berlin, Heidelberg, New York, 1985; Vol. 37.

(53) Rasmussen, Kj.; Engelsen, S. B.; Fabricius, J.; Rasmussen, B. . In *Recent Experimental and Computational Advances in Molecular Spectroscopy*; Fausto, R., Ed.; NATO ASI Series C: Mathematical and Physical Sciences; Kluwer Academic Publisher: Dordrecht, The Netherlands, 1993; Vol. 406, pp 381−419.

(54) Sabolović, J.; Tautermann, C. S.; Loerting, T.; Liedl, K. R. *Inorg. Chem.* **2003**, *42*, 2268–2279.

(55) Sabolović, J.; Liedl, K. R. *Inorg. Chem.* **1999**, *38*, 2764–2774.

(56) The charge values (e) used in the MM and MD simulations: Cu 1.30776; N −0.96611; C^{α} −0.12911, C^{β} −0.44111, C^{γ} and C^{δ} −0.50511, C′ 0.85999; $O_{carbonyl}$ −0.65811, $O_{carboxyl}$ −0.85611; H(N) 0.43789, H(C) 0.20889, O_{water} −0.8476, H_{water} 0.4238.

(57) Sabolović, J.; Raos, N. *Polyhedron* **1990**, *9*, 2419–2427.

(58) Sabolović, J. *Polyhedron* **1993**, *12*, 1107–1113.

(59) Sabolović, J.; Rasmussen, Kj. *Inorg. Chem.* **1995**, *34*, 1221–1232.

(60) Hay, B. P. *Coord. Chem. Rev.* **1993**, *126*, 177–236.
(61) Boeyens, J. C. A.; Comba., P. *Coord. Chem. Rev.* **2001**, *212* (1), 3–10.
(62) Deeth, R. J.; Anastasi, A.; Diedrich, C.; Randell, K. *Coord. Chem. Rev.* **2009**, *253*, 795–816.
(63) Bentz, A.; Comba., P.; Deeth, R. J.; Kerscher, M.; Seibold, B.; Wadepohl, H. *Inorg. Chem.* **2008**, *47*, 9518–9527.
(64) Williams, D. E. *Top. Curr. Phys.* **1981**, *26*, 3–40.
(65) Pietilä, L.-O.; Rasmussen, Kj. *J. Comput. Chem.* **1984**, *5*, 252–260.
(66) Lindahl, E.; Hess, B.; van der Spoel, D. *J. Mol. Model.* **2001**, *7*, 306–317.
(67) Berendsen, H. J. C.; van der Spoel, D.; van Drunen, R. *Comput. Phys. Commun.* **1995**, *91*, 43–56.
(68) D'Angelo, P.; Bottari, E.; Festa, M. R.; Nolting, H.-F.; Pavel, N. V. *J. Phys. Chem. B* **1998**, *102*, 3114–3122.
(69) Berendsen, H. J. C.; Postma, J. P. M.; van Gunsteren, W. F.; DiNola, A.; Haak, J. R. *J. Chem. Phys.* **1984**, *81*, 3684–3690.
(70) Miyamoto, S.; Kollman, P. A. *J. Comput. Chem.* **1992**, *13*, 952–962.
(71) One must note that there is no experimental evidence on the *cis*−*trans* isomerization mechanism of $Cu(aa)_2$ complexes in aqueous solution, whether it happens via chelate-ring twisting without breaking bonds, and/or via bond-breaking and bond-forming mechanism. The MD modeling results are based on the first mechanism as there is no reactive force field developed for $Cu(aa)_2$ complexes that may be suitable to treat bond-breaking and bond-making systems. However, whatever the mechanism is of the *cis*−*trans* isomerization in solution, the calculations done for $Cu(Gly)_2$ suggested the isomerization would happen at much longer time scale (the isomerization reaction rates were evaluated to be on the order from milliseconds to seconds)[37] than could be achievable by MD simulations. Thus, we supposed the isomerization mechanism should not influence the accomplished MD simulation results.
(72) The solubility measurements in aqueous solution at room temperature yielded the following values: 17.1 mg mL^{-1} and 18.2 mg mL^{-1} for initially synthesized powder and single crystals of *cis* $Cu(L\text{-}Val)_2 \cdot H_2O$, respectively; 16.1 mg mL^{-1} for thermally treated powder, and 13.8 mg mL^{-1} for *trans* $Cu(L\text{-}Val)_2$ single crystals. By dissolving 0.125 g of $Cu(L\text{-}Val)_2$ complex powder in 10 mL of water, there are 1314 water molecules per one $Cu(L\text{-}Val)_2$ molecule in the solution.
(73) Humphrey, W.; Dalke, A.; Schulten, K. *J. Molec. Graphics* **1996**, *14*, 33–38.